Locating the inflection point of frequency-dependent velocity dispersion by acoustic relaxation to identify gas mixtures

OPEN ACCESS
IOP Publishing
Measurement Science and Technology
Meas. Sci. Technol. **31** (2020) 115001 (11pp)
https://doi.org/10.1088/1361-6501/ab9375

Locating the inflection point of frequency-dependent velocity dispersion by acoustic relaxation to identify gas mixtures

Xiangqun Zhang[1,2], **Shu Wang**[1] **and Ming Zhu**[1]

[1] School of Electronic Information and Communications, Huazhong University of Science and Technology, Wuhan 430074, People's Republic of China
[2] School of Information Engineering, Xuchang University, Xuchang 461000, People's Republic of China

E-mail: zhuming@mail.hust.edu.cn

Received 30 September 2019, revised 11 May 2020
Accepted for publication 15 May 2020
Published 14 August 2020

Abstract

Measuring adiabatic sound speed is an effective method to characterize gases with different molecular weights because sound speed mainly depends on molecular weight at a given temperature. However, it is still a challenge to apply this method to different gas mixtures with similar or even the same sound speeds. Acoustic relaxation in gases may overcome this challenge because sound speed becomes dispersive due to frequency-dependent heat capacity. Based on our previous work on reconstructing acoustic velocity dispersion with a simple measurement method, in this paper, we propose capturing the inflection point of velocity dispersion to identify gas mixtures. Standard detection areas are constructed using the theoretical location of the inflection point scaled by the acoustic velocity and relaxation frequency with different temperatures for target gases. The captured inflection point is located in the detection areas to obtain gas compositions. Thus, gas mixtures with the same molecular weights, such as 86.9% CO_2–13.1% N_2, 95% CO_2–5% H_2 and 95% CO_2–5% pH_2, can be differentiated using our method from only their acoustic velocities. The results show that the maximum absolute error of the compositions for CO_2 can be effectively reduced from 3.8% to 0.2% by our temperature correction function. Therefore, the proposed method can identify gas mixtures qualitatively and quantitatively by only measuring acoustic velocity.

Supplementary material for this article is available online

Keywords: measurement of acoustic velocity, gas detection, acoustic relaxation, acoustic velocity dispersion, inflection point

(Some figures may appear in colour only in the online journal)

1. Introduction

The measurement of adiabatic sound speed is an effective method to determine the composition of gaseous mixtures. Thus, gas sensing by sound speed has several advantages, such as low-cost [1], high reliability [2, 3], fast response [4], and non-necessity of calibration [5], compared to other gas sensing methods, such as electrochemistry [6] and laser sensing

[7, 8]. To determine the compositions of gas mixtures using sound speed, different schemes and techniques have been successfully implemented. Witschi and Haber [9] first detected the presence of hydrogen or methane in underground mine air through the change of sound speed. Based on Haber's method, Garrett [10] suggested an acoustical gas analyzer for hydrogen and methane with high accuracy and precision by electronic temperature compensation. For complete automation, Hallewell *et al* [11] developed an online monitor to reveal small fluctuations in the compositions of binary gas mixtures from ultrasonic measurement. In summary, the above methods that used sound speed can identify only binary gas with low selectivity. Some researchers aimed to detect ranges of sound speed for more than two components. Lueptow and Phillips [5] determined the combustion quality of natural gas using the fact that the sound speed of CH_4 is higher than that of C_2H_6, C_3H_8, CO_2 and N_2; Zipser and Wächter [12] compared the ratio of anisentropic sound speed to isentropic speed to distinguish ternary gas mixtures and improve selectivity. All of the above methods have achieved positive results for identifying gas mixtures. However, they only sensed the sound speed of gas mixtures from different molecular weights and failed to acquire more molecular information. Thus, for different gas mixtures with the same molecular weights, such as 95% CO_2–5% pH_2, 95% CO_2–5% H_2, and 86.9% CO_2–13.1% N_2, gas sensing by sound speed has been a challenge for almost a century.

According to acoustic relaxation theory, acoustic velocity changes not only with molecular weight but also with the heat capacity ratio of gas mixtures, and it becomes dispersive from frequency-dependent heat capacity [13]. Different gas mixtures with the same molecular weights may have the same acoustic velocities but different relaxation frequencies, at which acoustic relaxation happens most notably. Because each molecule has a unique relaxation mode, molecular relaxation information can be employed to identify gas compositions [14, 15]. For example, Hu *et al* [15] located absorption spectral peaks to detect gas mixtures by jointly measuring the attenuation coefficient and sound speed, which is based on Zhang *et al*'s [16] two-frequency acoustic measurements. Liu *et al* [17, 18] verified Hu *et al*'s simplified theory by extracting molecular internal effective specific heat. We provide a mixed rotational and vibrational relaxation model of hydrogen gas mixtures and decouple the multiple rotational relaxation into a group of singe relaxation processes to improve the accuracy of ternary gas mixture sensing based on acoustic velocity and absorption [19, 20]. However, compared with acoustic velocity, the absorption coefficient has a large measurement error in the order of 5% and results in low detection sensitivity [21]. Recently, we proposed a simple measurement method to reconstruct acoustic velocity dispersion by only measuring acoustic velocities at several fixed frequencies [22]. On the S-shaped curve of frequency-dependent velocity dispersion due to acoustic relaxation processes, we find the inflection point of the dispersion curve to determine the molecular weight and the relaxation frequency at the same time. Thus, by combining our simple measurement of acoustic dispersion [22] and the mixed rotational and vibrational relaxation model [19], we propose a method to characterize gas compositions by locating the inflection point in this paper.

The remainder of this paper is organized as follows. In section 2, we discuss the location of the inflection point of the velocity dispersion in gas scaled by acoustic velocity, acoustic frequency, and temperature to demonstrate that it can be used to identify gas mixtures. In section 3, we obtain the inflection point from measured velocities by reconstructing the velocity dispersion to distinguish gas mixtures with similar, or even the same, acoustic velocities. In section 4, we analyze the detection uncertainty from the velocity measurement error and provide a temperature correction approach. In section 5, we present some concluding remarks.

2. Gas composition sensing theory based on the location of the inflection point of acoustic velocity dispersion

Acoustic propagation in gases can be characterized by a complex-valued effective wave number $k^{\mathrm{eff}}(\omega)$ and the effective thermodynamic sound speed c_e; both of them are expressed as [23]

$$k^{\mathrm{eff}}(\omega) = \frac{\omega}{V(\omega)} - \mathrm{i}\alpha_{\mathrm{r}}(\omega) = \frac{\omega}{c_e}, \tag{1}$$

where $\alpha_{\mathrm{r}}(\omega)$ is the relaxation absorption and $V(\omega)$ is acoustic velocity. $V(\omega)$ is defined as

$$V(\omega) = \sqrt{\frac{RT\gamma(\omega)}{M}}, \tag{2}$$

where M and T are the molar mass and temperature of the gas, respectively; R is the universal gas constant. $\gamma(\omega) = \left(C_{\mathrm{V}}^{\mathrm{eff}}(\omega) + R\right)/C_{\mathrm{V}}^{\mathrm{eff}}(\omega)$ is the heat capacity ratio and $\omega = 2\pi f$ is the acoustic angular frequency. Under adiabatic conditions, $C_{\mathrm{V}}^{\mathrm{eff}}(\omega)$ has a fixed value for each kind of gas molecule, meaning $\gamma(\omega)$ has traditionally been divided into three categories based on whether the gas is monatomic, or composed by diatomic, or polyatomic molecules. Based on the fixed heat capacity ratio and average molar mass, traditional methods analyze the compositions of binary gas mixtures by measuring sound speed [9–11]. However, this analysis cannot be applied to multi-component gas mixtures or gas mixtures with the same sound speeds because of the ill-posedness of the mathematical problem.

2.1. Inflection points of acoustic velocity dispersions for gases

According to acoustic relaxation theory, $C_{\mathrm{V}}^{\mathrm{eff}}(\omega)$ reflects the footprint of the molecular relaxation of gases [24]. For a gas mixture with W kinds of molecules, including N types of vibrational modes, $C_{\mathrm{V}}^{\mathrm{eff}}(\omega)$ changes with acoustic frequency and is expressed as [25]

$$C_{\mathrm{V}}^{\mathrm{eff}}(\omega) = C_{\mathrm{V}}^{\infty} + \sum_{i=1}^{N} \frac{C_i^{\mathrm{int}}}{1 + \mathrm{i}\omega\tau_i}, C_{\mathrm{V}}^{\infty} = \sum_{l=1}^{W} a_l C_l^{\infty}, \sum_{l=1}^{W} a_l = 1, \tag{3}$$

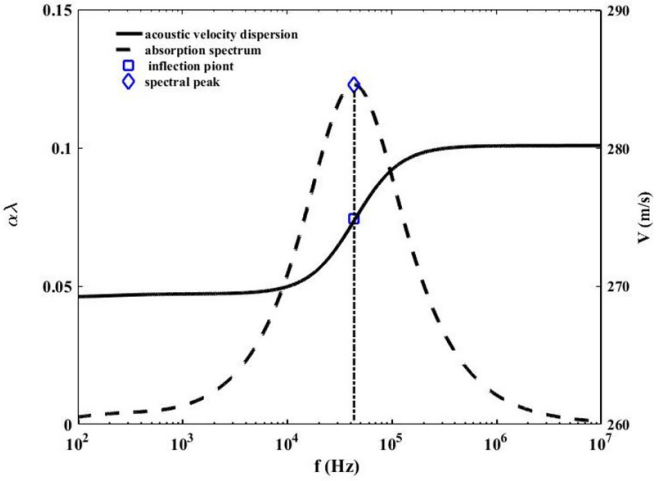

Figure 1. Frequency dependences of acoustic velocity and absorption spectrum for CO_2 at $T = 297$ K, which were calculated from Zhang's model [19].

where C_V^∞ and C_l^∞ are the translational and rotational specific heats of the gas mixture and molecule l, respectively; a_l is the mole fraction of gas molecule l; $C_i^{\text{int}}$and τ_i are the vibrational specific heat and relaxation time of the ith single-relaxation process.

On the one hand, in equation (1) the imaginary part of $k^{\text{eff}}(\omega)$ determines the relaxation absorption $\alpha_r(\omega)$, which is conventionally represented by the dimensionless absorption coefficient $\alpha_r(\omega)\lambda$ [26], where is the acoustic wavelength. Thus $\alpha_r(\omega)\lambda$ is given by

$$\alpha_r(\omega)\lambda = -2\pi\frac{\text{Im}\left(k^{\text{eff}}(\omega)\right)}{\text{Re}\left(k^{\text{eff}}(\omega)\right)}. \tag{4}$$

Figure 1 shows the variation of $\alpha_r(\omega)\lambda$ versus frequency for gaseous CO_2, which results from the molecular vibrational–vibrational and vibrational–translational relaxation processes [21]. The bell-shape absorption spectrum is characterized by the peak amplitude reflecting the relaxation strength. The corresponding frequency is the effective relaxation frequency, which is the reciprocal of the relaxation time. As a result, the peak contains the relaxation characteristics of gas mixtures. On this basis, Hu *et al* [15] employed the location of the spectral peak to identify the gas compositions of CO_2–N_2 and CH_4–N_2 mixtures.

On the other hand, based on equations (1) and (2), the real part of $k^{\text{eff}}(\omega)$ determines the acoustic velocity $V(\omega)$. $V(\omega)$ can be expressed as a function of the effective isochoric molar heat capacity $C_V^{\text{eff}}(\omega)$:

$$V(\omega) = \sqrt{\frac{RT}{M}\left(1 + \frac{R}{C_V^{\text{eff}}(\omega)}\right)}. \tag{5}$$

Figure 1 also plots the variation of $V(\omega)$ against frequency, which also results from the same molecular relaxation processes as $\alpha_r(\omega)\lambda$ [21]. Clearly, $V(\omega)$ monotonically increases with increasing frequency f on the S-shape acoustic velocity dispersion curve. The velocity V_m of the inflection point on the curve can be defined as [27]

$$V_m = \sqrt{\left(V^2(\infty) + V^2(0)\right)/2}, \tag{6}$$

where $V^2(0)$ and $V^2(\infty)$ are the minimum and maximum values of the squared acoustic velocities in the lowest and highest limits of acoustic frequencies, respectively. $V^2(0)$ and $V^2(\infty)$ are obtained from

$$V^2(0) = \frac{RT}{M}\left(1 + \frac{R}{C_V^{\text{eff}}(0)}\right), V^2(\infty) = \frac{RT}{M}\left(1 + \frac{R}{C_V^{\text{eff}}(\infty)}\right), \tag{7}$$

where $C_V^{\text{eff}}(0)$ denotes the sum of the external and internal isochoric molar heat capacities, and $C_V^{\text{eff}}(\infty)$ represents the external isochoric molar heat capacity of the gas mixtures.

In figure 1, the frequency f_m of the inflection point has the same value as the absorption spectrum peak because both represent the effective relaxation frequency of the acoustic relaxation process. The inflection point is a unique point on the acoustic velocity dispersion curve and carries the information of the relaxation frequencies. Similar to Hu *et al*'s method, which employed the location of the spectral peak to detect gas compositions [15], we propose using the location of the inflection point to identify gas compositions.

2.2. Locations of the inflection points of acoustic velocity dispersion for gas sensing

To determine the composition of a gas mixture, the measurement of the inflection point must be compared with the prediction of a theoretical model. For most gases, molecular vibrational relaxation dominates the relaxation processes, and the rotational relaxation is regarded as constant at ambient temperature [23, 24, 28, 29]. However, for hydrogen, molecular rotational relaxation plays a key role in the relaxation processes, while vibrational relaxation is negligible at ambient temperature [30]. Recently, combining Zhang's vibrational model for gas mixtures such as CH_4, N_2, CO_2 [25], we proposed a mixed rotational and vibrational relaxation model to calculate the acoustic characteristic of hydrogen gas mixtures [19]. Based on the mixed relaxation model [19], theoretical acoustic velocity dispersion in this paper is obtained and a theoretical inflection point is acquired for gas mixtures. The theoretical detection areas of these inflection points are constructed at different temperatures, as shown in figure 2. The green curves refer to the influence of temperature on the locations of the inflection points at a constant composition of the gas mixtures. The blue and red curves indicate how the locations of the inflection points vary with the compositions of gas mixtures at fixed temperatures of 273 K and 323 K, respectively.

Gas mixtures with different compositions have different inflection point locations. The effective detection area of CO_2–N_2 is located at the bottom and left of figure 2, while that of CH_4–N_2 is located at the top and left. Meanwhile, the effective detection area of CO_2–H_2 is located at the bottom and right, and that of CH_4–N_2 is located at the top and right. Clearly, gas mixtures of CH_4–N_2, CO_2–N_2, CH_4–H_2, and CO_2–H_2 can

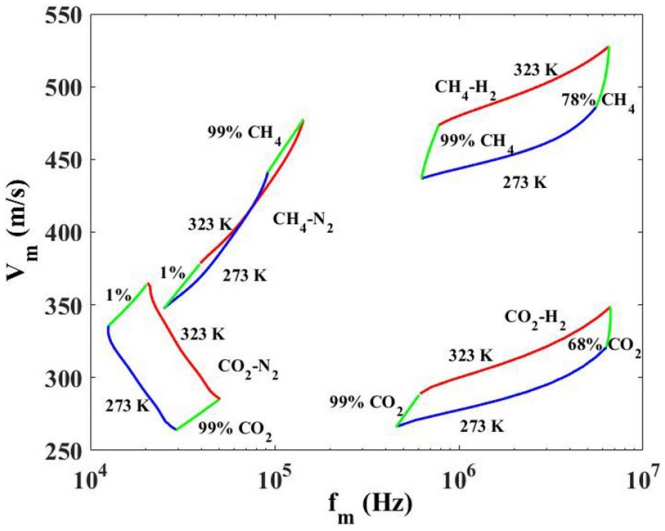

Figure 2. Effective detection areas of the inflection points for gas mixtures with concentration increments of 0.1% and temperature increments of 0.1 K. The concentrations of CO_2 and CH_4 in N_2 vary from 1%99%; the concentrations of CO_2 and CH_4 in H_2 vary from 68%99% and from 78%99%, respectively.

be qualitatively identified by their respective effective detection areas. By comparison, it can be seen from figure 2 that the acoustic velocity of gas mixtures CO_2–N_2 ranges from approximately 262 m s^{-1} to 370 m s^{-1} while that of gas mixtures CO_2–H_2 is, similarly, approximately 267 m s^{-1} to 350 m s^{-1}. The corresponding relaxation frequency of CO_2–N_2 varies from approximately 11 kHz–52 kHz, while that of CO_2–H_2 ranges from 460 kHz–6670 kHz. Due to their overlapping ranges of acoustic velocity, traditional methods fail to identify the gas mixtures, considering only sound speed, but the different compositions of CO_2–N_2 and CO_2–H_2 give them independent effective inflection point detection areas, which can be used to distinguish them.

3. Identification procedure for gas mixtures based on the location of the inflection point

3.1. Obtaining the inflection point by simple measurement method

To apply our proposed method to practical industry, simple measurement is necessary. Conventional methods [31–33] measure the acoustic velocities over a wide frequency range to obtain the acoustic velocity dispersion. However, it is impractical to operate this by changing the frequency in real time due to a longer measurement procedure and numerous transducers. To overcome this problem, we recently developed a simple measurement approach to reconstruct the whole acoustic velocity dispersion of gas mixtures by solely measuring acoustic velocities at 3–5 frequencies [22]. The frequency-dependent acoustic velocity dispersion of the multi-relaxation processes

Table 1. The type B uncertainty contributions of instruments.

Sources	Uncertainty
Delay time	0.03 us
Acoustic path length	0.0005 mm
Temperature	0.03 K
Pressure	0.000029 MPa
Test gas mixtures	2%

of gas mixtures can be expressed as [22]

$$V^2(\omega) = V^2(\infty)\left(1 - \sum_{i=1}^{N} \frac{\varepsilon_i}{1+\omega^2\tau_i^2}\right), \tag{8}$$

where τ_i and ε_i are the relaxation time and relaxation strength of the ith single relaxation process of gas mixtures, respectively. In equation (8), for a single relaxation process, $V(\omega)$ can be expressed as a function of $V(\infty)$, ε, and τ. Because the vast majority of multi-relaxation processes of gases represent one primary relaxation process, $V(\infty)$, ε and τ can be obtained to reconstruct $V(\omega)$ in practice by measuring the acoustic velocities at three frequencies [22]. Therefore, one can determine the location of the inflection point from reconstructed acoustic velocity dispersion using equations (5) and (8).

3.2. Experimental apparatus

The prototype sensor shown in figure 3(a) is used to measure the acoustic velocities of gases. The sensor has six pairs of transmitterreceiver transducers matching frequencies of 25 kHz, 40 kHz, 75 kHz, 100 kHz, 300 kHz, and 400 kHz. The stepper motor drives the translation stage to move the emitter, while the receiver was kept stationary.

The experimental apparatus shown in figure 3(b) is composed of the sensor, the chamber, control panel, gas bottle, vacuum pump (on the back) and measurement instruments. The sensor in figure 3(a) is sealed in the chamber with a diameter of 400 mm and a length of 620 mm. The chamber is made of cylindrical stainless steel, and it can sustain a pressure from −0.001 MPa to 2.5 MPa. The control panel turns the valves of the pipeline on or off to control gases in or out of the chamber. The test gas mixtures 86.9% CO_2–13.1% N_2, supplied by Newruide Special Gas Company in China, were mixed by CO_2 and N_2 with a claimed purity of 99.999%. The vacuum pump is used to evacuate gases in the chamber, where the degree of vacuum is on the order of −0.001 MPa. Two digital pressure measurements are used to sense pressure, one with a range from 0100 kPa works for negative pressure and the other with a range from 0 MPa3 MPa is for positive pressure. One digital thermometer with a probe is placed near the receiver and the other is near the door of the chamber, which were calibrated on ITS-90. The type B uncertainty contributions of the instruments are estimated and shown in table 1. Three representative points on the acoustic velocity dispersion curve are selected and the contribution of the pressure to the combined uncertainty of the acoustic velocity is estimated in table 2.

Table 2. An estimate of the contribution of the pressure uncertainty to the combined uncertainty of the acoustic velocity.

Frequency (kHz)	Pressure (MPa)	Uncertainty of the pressure (MPa)	Final frequency (kHz)	Combined uncertainty of acoustic velocity (m s^{-1})
25	0.2	±0.001	12.5	±0.002
40	0.1	±0.001	40	±0.02
400	0.08	±0.001	500	±0.0015

Note: Final frequency (kHz): acoustic velocity at the corresponding frequency on the acoustic velocity dispersion curve, which is equal to frequency with kHz over pressure with 0.1 MPa.

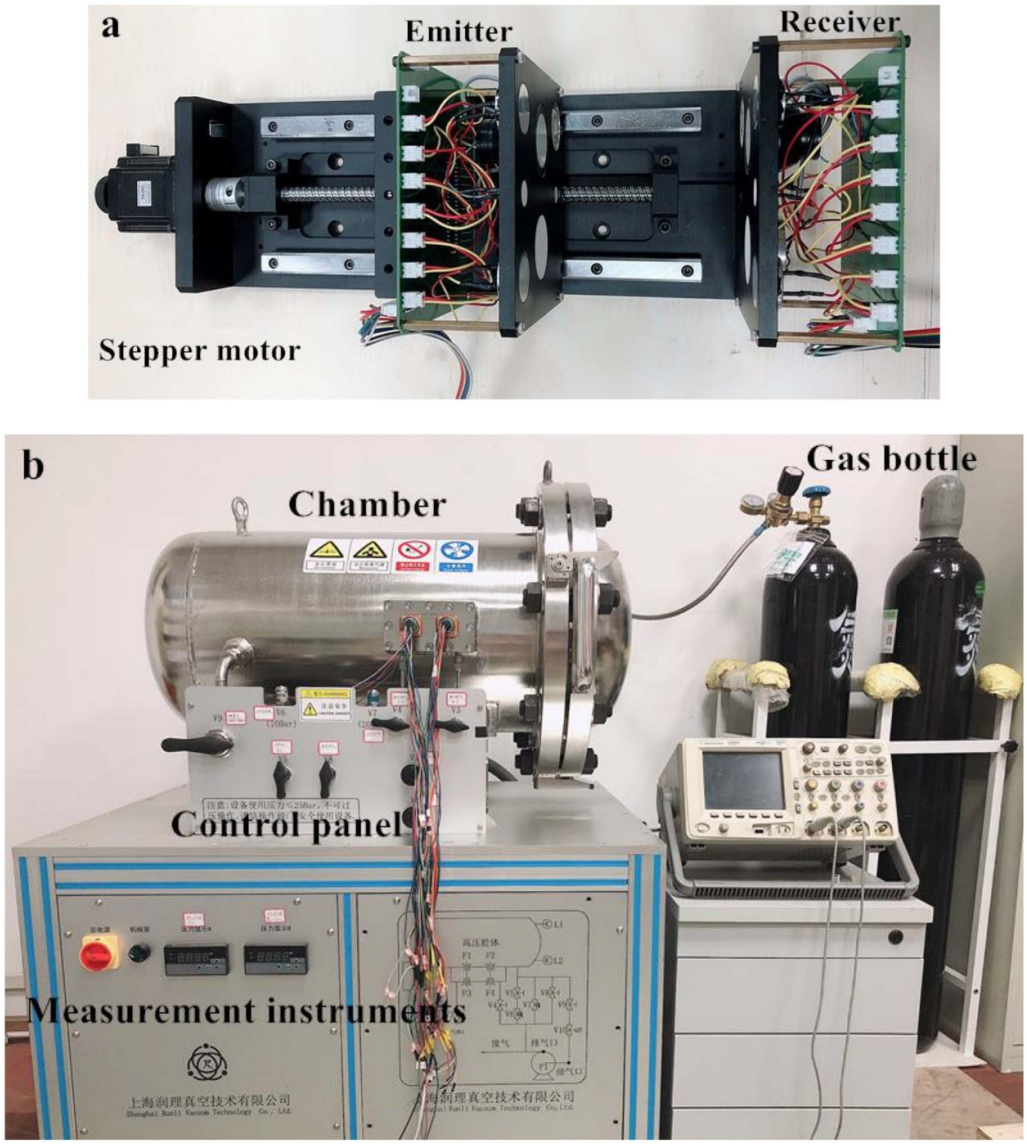

Figure 3. (a) Prototype sensor. (b) Experimental apparatus.

Trusler *et al* [34–37] accurately measured the speed of sound in several gases at variable pressures along different isotherms by means of an interferometer or resonator. In contrast, we measured acoustic velocity directly by moving the distance of the emitter and relative delay time between the maximum wave peaks of the receiver over a wide frequency/pressure range, where the accuracy is lower than that of Trusler's method due to experimental limits. A similar measurement procedure was carried out by Ejakov *et al* [23], the only difference being that they measured acoustic attenuation but we measured acoustic velocity. According to the relaxation theory of gases, lowering the pressure is equal to raising the frequency [23]. One usually changes the gas pressure to broaden the measured frequency range to obtain adequate experiment

Table 3. The final frequencies (kHz) at the ratio of frequencypressure are listed.

Frequency (kHz)	Pressure (MPa)						
	0.06	0.08	0.1	0.2	0.4	0.6	0.8
25	41.667	31.25	25	12.5	6.25	4.1667	3.125
40	66.667	50	40	20	10	6.667	5
75	125	93.75	75	37.5	18.75	12.5	9.375
100	166.667	125	100	50	25	16.667	12.5
300	500	375	300	150	75	50	37.5
400	666.667	500	400	200	100	66.667	50

Note: Final frequency (kHz): acoustic velocity at the corresponding frequency on the acoustic velocity dispersion curve, which is equal to frequency with kHz over pressure with 0.1 MPa.

data. Consequently, the acoustic velocity dispersion is plotted as the frequency/pressure ratio *f/p*. In our experiment, at seven different pressures from 0.06 MPa– 0.8 MPa and six frequencies from 25 kHz–400 kHz, the expanded frequency range was from 3.125 kHz–666.6 kHz, as shown in table 3. Some ratios of frequency/pressure were the same, for example, one final frequency was 66.667 kHz at a ratio of frequency/pressure 40 kHz/0.06 MPa; the other was 66.667 kHz at a ratio of 400 kHz/0.6 MPa, which were marked in the same color in table 3. Velocities at the same frequency-pressure ratio *f/p* were averaged. We did experiment four times at a temperature of about 303.1 K to 303.3 K. The experimental data (symbols '◯') for gas mixture 86.9% CO_2–13.1% N_2 is shown in figure 4(a). The type A uncertainty of velocity at each frequency is shown in table 4. Comparisons with our estimator of type A uncertainty of velocity at each frequency, the type B uncertainty contributions in table 1, are negligibly small and can be safely neglected. The error bars of acoustic velocities shown in figure 4(a) mainly arise from type A uncertainty contribution. The acoustic velocity with an overall standard uncertainty of 0.36 m s^{-1} is approximately estimated. More details for the experiment and measurement are shown in a supplementary file online.

Now we obtain the inflection points on the acoustic velocity dispersion curves from the experimental data. On the one hand, the raw data $V_1 = 278.55$ m s^{-1}, $V_2 = 283.33$ m s^{-1}, and $V_3 = 290.00$ m s^{-1} (the blue symbols '□' in figure 4(a)) at the corresponding frequencies of 4.167 kHz, 40 kHz, and 500 kHz are used to reconstruct the acoustic velocity dispersion of gas mixture 86.9% CO_2–13.1% N_2. Based on the reconstructed dispersion (the black curve), the inflection point ($f_m = 46.777$ kHz and $V_m = 284.28$ m s^{-1}) is calculated and represented by the red symbol '■' in figure 4(a). On the other hand, gas mixtures of 95% CO_2–5% H_2 and 95% CO_2–5% pH_2 at $T = 303.15$ K are considered. The symbols '◯' and '△' in figure 4(b) represent the experimental data of gas mixtures 95% CO_2–5% H_2 and 95% CO_2–5% pH_2 from Behnen *et al* [38], respectively. The blue symbols '□' represent the selected points for reconstructing velocity dispersion, which are $V_1 = 279.12$ m s^{-1}, $V_2 = 283.02$ m s^{-1}, and $V_3 = 290.64$ m s^{-1} at the frequencies of 120 kHz, 500 kHz, and 6 MHz, respectively. The red symbol '■' denotes the synthesized inflection point ($f_m = 699$ kHz and $V_m = 284.8$ m s^{-1})

Table 4. The type A uncertainty contribution of acoustic velocity at final frequency in figure 4(a).

Frequency (kHz)	Acoustic velocity (m s^{-1})	Uncertainty (m s^{-1})	Frequency (kHz)	Acoustic velocity (m s^{-1})	Uncertainty (m s^{-1})
3.125	277.94	0.43	41.667	286.81	0.88
4.167	278.48	0.37	50	284.39	0.34
5	277.43	0.35	66.667	284.77	0.88
6.25	279.82	0.22	75	286.75	0.32
6.667	278.63	0.25	93.75	287.60	0.97
9.375	277.30	0.19	100	286.99	0.25
10	279.38	0.25	125	288.55	0.64
12.5	279.00	0.37	150	289.03	0.29
16.667	278.93	0.12	166.667	289.27	0.38
18.75	281.19	0.23	200	288.79	0.30
20	280.81	0.27	300	290.29	0.47
25	283.06	0.86	375	290.50	0.18
31.25	283.95	0.65	400	290.02	0.10
37.5	282.55	0.46	500	290.36	0.09
40	283.33	0.34	666.667	290.43	0.18

Note: Final frequency (kHz): acoustic velocity at the corresponding frequency on the acoustic velocity dispersion curve, which is equal to frequency with kHz over pressure with 0.1 MPa.

from the acoustic velocity dispersion of 95% CO_2–5% H_2. For comparison, the black symbol '■' denotes the inflection point of 95% CO_2–5% pH_2.

3.3. Identifying the compositions of the gas mixtures with the same molecular weights

Next, we begin to identify the above gas mixtures qualitatively and quantitatively using the locations of the inflection points. First, we identify gas mixtures qualitatively by locating the inflection points of gas mixtures in the effective detection areas of figure 2. If the location of the inflection point in figure 4(a) is in the effective detection area of CO_2–N_2, the unknown gas mixture is identified as CO_2–N_2; meanwhile, if the location of the inflection point in figure 4(b) is in the effective detection area of CO_2–H_2, it is identified as CO_2–H_2. Secondly, the composition of the gas mixtures is determined quantitatively as follows. Figure 5 depicts detailed locations of the inflection points for gas mixtures CO_2–N_2, CO_2–pH_2, and CO_2–H_2 in the detection areas. The inflection point ($f_m = 46.77$ kHz and $V_m = 284.28$ m s^{-1}, red '□') in figure 5(a) corresponds to the symbol '■' in figure 4(a). In figure 5(a), one dotted curve from the constant temperature 303.15 K and the other from the constant concentration 86.9% CO_2–13.1% N_2 of gas mixtures intersect at the inflection point, allowing us to univocally determine the mixture composition and the gas temperature. Similarly, the inflection point ($f_m = 699$ kHz and $V_m = 284.8$ m s^{-1}, red '□') in figure 5(b) corresponds to the red symbol '■' in figure 4(b). One red curve from $T = 303.15$ K and the other from constant concentration 95% CO_2–5% H_2 intersect at the inflection point. We remark, by comparison of figures 4(a) and (b), that the gas mixtures 86.9% CO_2–13.1% N_2 and 95% CO_2–5% H_2 have similar acoustic velocity values at the same temperature

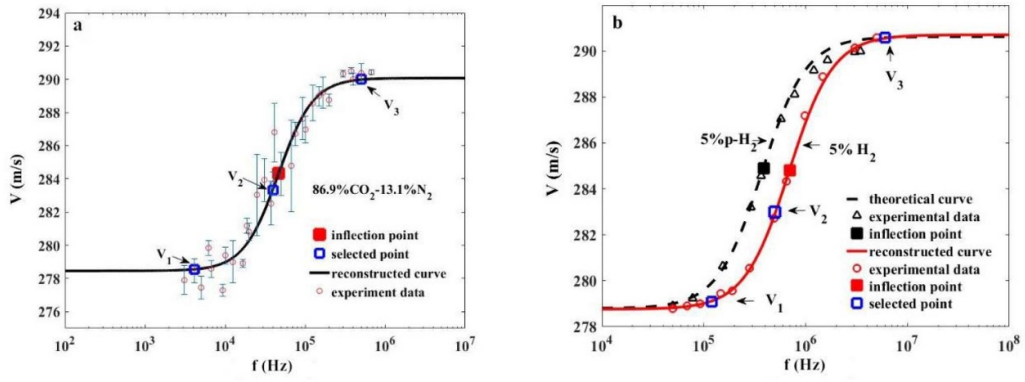

Figure 4. (a) Acoustic velocities with error bars from our experiment apparatus and the synthesized inflection point for 86.9% CO_2–13.1% N_2. (b) The synthesized inflection points from acoustic velocity dispersions for 95% CO_2–5% H_2 and 95% $CO_2$5% H_2 from Behnen *et al* [38].

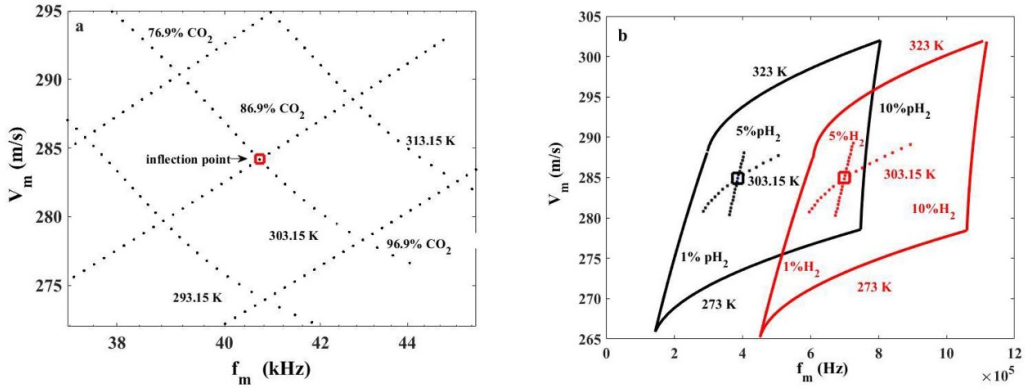

Figure 5. Locating the inflection point in the detection area. (a) Gas mixtures 86.9% CO_2–13.1% H_2. (b) Black '□': the inflection point for 95% CO_2—-5% pH_2 and red '□': the inflection point for 95% CO_2–5% H_2.

because they have the same molecular weight, and traditional methods struggle to differentiate them. However, our proposed method can distinguish them because different molecules and compositions of gas mixtures result in different relaxation frequencies.

H_2 and pH_2 are spin isomers with exactly the same molecular weight. At ambient temperature, the difference between the ideal-gas heat capacity ratio of pH_2 and H_2 is small (about 2%) [39]. Both the same molecular weight and a small difference in heat capacity ratio lead to about 0.1 m s^{-1} difference of acoustic velocities between 95% CO_2–5% pH_2 and 95% CO_2–5% H_2. The above coincidence cannot be distinguished by traditional gas sensing methods using sound speed only. However, our method can differentiate 95% CO_2–5% pH_2 and 95% CO_2–5% H_2 by their different relaxation frequencies. The frequency of the inflection point for the former mixture is 388 kHz which falls in the effective detection area of CO_2–pH_2 (black lines in figure 5(b)), while that of the latter is 699 kHz falling in the area of CO_2–H_2 (red lines in figure 5(b)). Clearly, it is still difficult to identify the gas mixtures because some part of the effective detection area of CO_2–pH_2 overlaps with that of CO_2–H_2. However, we can eliminate the incorrect result. In the effective detection area of CO_2–H_2, the location of the inflection point of 95% CO_2–5% H_2 (red '□' in figure 5(b)) is also identified as 90.5% CO_2–9.5% pH_2 at $T = 291$ K. By comparing $T = 291$ K with the ambient temperature, i.e. 303.15 K (measured by a precise thermometer), the final result is gas mixture 95% CO_2–5% H_2 and not 90.5% CO_2–9.5% pH_2. Therefore, using the locations of the inflection points, one can analyze the compositions of gas mixtures with similar or even the same acoustic velocities.

4. Analysis of measurement errors and correction

4.1. Analysis of the measurement errors

In this section, we evaluate the influence of one possible error in the determination of the acoustic velocity on the location of the inflection point. According to the reconstruction method of acoustic velocity dispersion, the inflection point on velocity dispersion for most gases can be obtained by measuring acoustic velocities at three frequencies [22]. We first suppose that there is one measurement error at the three frequencies, and then assume that there are two measurement errors at the three frequencies. If there are three measurement errors at respective frequencies, for example, all the velocities are too large or too small. In this situation, the obtained velocity dispersion is likely to overlap with the other velocity dispersion and cannot

be corrected. Thus, three measurement errors at three frequencies are not considered here. The error correction and analysis in this section all are based on the gas mixtures 86.9% CO_2–13.1% N_2 at the temperature 303.15 K.

Suppose that the measurement error of acoustic velocity comes from one of three frequencies f_1, f_2 and f_3, while others have no errors. Figure 6(a) considers the case when V_1 at $f_1 = 4.667$ kHz may be in error by about 1%, which is the worst case of measurement error, as shown in figure 4(a), while figure 6(b) considers the case when V_2 at $f_2 = 40$ kHz is in error by the same relative amount. It can be observed from figure 6(a) that the position of the obtained inflection point increases from left to right with an increase in V_1. Therefore, a larger V_1 leads to a larger V_m. Similarly, the effect of a measurement error affecting V_3 would produce the same effect with the same trend and is not plotted in figure 6 to avoid repetition. In contrast, as V_2 increases and decreases in figure 6(b), the velocity value V_m of the inflection point remains unchanged, while the corresponding relaxation frequency f_m slightly decreases and increases, respectively. This is because the velocity value of the inflection point depends only on the sum of $V^2(\infty)$ and $V^2(0)$.

According to the identification procedure, the consequence of velocity errors may lead to errors in the determination of the composition of the mixture and the temperature which are calculated from the dispersion model. Figure 7 shows how the relative detection errors of the gas concentration ξ (86.9% CO_2 in gas mixtures 86.9% CO_2–13.1% N_2) and those of the calculated temperature T by the dispersion model to the real temperature vary with relative measurement errors of the acoustic velocities V_1 and V_2, respectively. The relative error of V_1 is proportional to the errors of ξ and T in figure 7(a), while that of V_2 is inversely proportional to those of ξ and T in figure 7(b). The relative measurement error of V_3 has the same tendency as that of V_1. Furthermore, it can be observed from figure 7 that the relationship between the relative error of acoustic velocity and that of temperature is approximately linear. According to computer analysis, the relationship between the relative error of velocity ΔV and that of temperature ΔT is

$$\Delta V = \sqrt{\Delta T}/1000. \tag{9}$$

In the following section, based on equation (9), we use the difference between the temperature determined by the dispersion model and the temperature measured by a thermometer to correct the measurement error of the acoustic velocities of the gas mixtures.

4.2. Correction for measurement error

The correction procedure where the measurement error arises from one of three frequencies is discussed in figure 8(a). Three acoustic velocities of $V_1 = 279.3$ m s^{-1} at $f_1 = 4.167$ kHz, $V_2 = 283.3$ m s^{-1} at $f_2 = 40$ kHz, and $V_3 = 290.1$ m s^{-1} at $f_3 = 500$ kHz ('•' in figure 8(a)), which come from our raw experimental data, are used to reconstruct the acoustic velocity dispersion. The corresponding inflection point ($f_m = 52.66$ kHz and $V_m = 284.77$ m s^{-1}) is calculated from the reconstructed velocity dispersion and shown as the farthest '◯' from '◊' in figure 8(b). By locating this inflection point in the detection area of CO_2–N_2, gas mixture 92.0% CO_2–8.0% N_2 at $T = 310.6$ K is obtained. Clearly, the identification result is incorrect by comparing the temperature of 310.6 K with the real one of 303.15 K. First, suppose the measurement error comes from V_1 at f_1 since we do not know at which frequency point the measurement error occurs. The relative error ΔT between the obtained 310.6 K and real 303.15 K is 2.46%. The corresponding correction factor $\Delta V = 0.016\%$ for V_1 is calculated by equation (9). After V_1 decreases by the correction factor of ΔV, the new inflection point is synthesized. By repeating the correction procedure iteratively, V_1 can be continuously corrected until ΔT converges to zero. The symbols '◯' in figure 8(b) reflect the traces of the corresponding inflection points and the arrow refers to the correction direction. The final detection result is gas mixture 86.9% CO_2–13.1% N_2 at temperature 303.6 K. Secondly, suppose that the measurement errors from V_2 at f_2, and V_3 at f_3 are also considered, respectively. The traces of the corresponding inflection points during the temperature correction processes are shown as '+' and '□' in figure 8(b), respectively, and the detection results are listed in table 5. Therefore, for the situation of one measurement error, even if one does not know which particular measurement point is affected by an error, our correction method can restrict the maximum absolute error to 0.2% based on the volume concentration of CO_2.

To further demonstrate the correction approach, the measurement errors of acoustic velocities from two of three frequencies are considered. $V_2 = 283.3$ m s^{-1} at $f_2 = 40$ kHz (no error), both $V_1 = 277.5$ m s^{-1} at $f_1 = 3.125$ kHz and $V_3 = 289.4$ m s^{-1} at $f_3 = 500$ kHz with errors are shown as red symbols '*' in figure 9(a), which also come from our raw experimental data for gas mixtures 86.9% CO_2—-13.1% N_2 at $T = 303.15$ K. The initial detection result is 83.6% CO_2–16.4% N_2 at $T = 294.4$ K. Because we do not know which two of the three are errors, suppose firstly the measurement errors come from V_1 and V_3. Both V_1 and V_3 are increased by the same factor of ΔV by comparing 294.4 K with the real $T = 303.15$ K, and a new inflection point is synthesized. Iterating the correction steps, the traces of the corresponding inflection points are shown as '*' in figure 9(b). The final location of the inflection point determines that the gas mixture is 86.8% CO_2–13.2% N_2 as shown in table 6. The measurement errors from two situations of V_2 and V_3, V_1 and V_2 are also considered. Their traces of the corresponding inflection points are shown as symbols '△' and '+' in figure 9(b) and the results are listed in table 6.

In conclusion, whether there is one or two measurement errors of acoustic velocities at three frequencies and whether or not one knows where the measurement errors occur, our correction method based on temperature can improve the detection results. A similar temperature correction was conducted to determine gas mixture 40% CO_2–60% N_2 at $T = 293.7$ K [15]. Compared with Hu *et al's* [15] detection error of 4.75% for a CO_2 composition, our maximum abso-

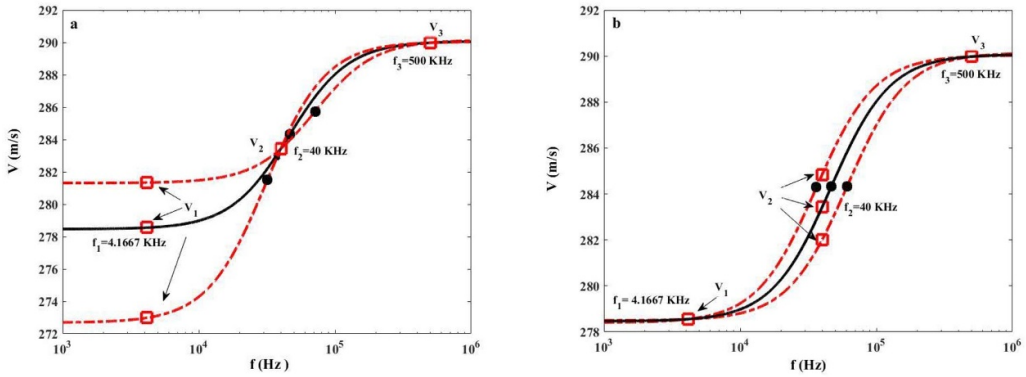

Figure 6. Locations of the inflection points depending on variations of V_1 at $f_1 = 4.667$ kHz and V_2 at $f_2 = 40$ kHz for 86.9% CO_2–13.1% N_2 at $T = 303.15$ K; the dashed and solid curves represent the reconstructed acoustic velocity dispersion with errors and without errors, respectively. •: locations of the inflection points; □: selected points for reconstructing acoustic velocity dispersion.

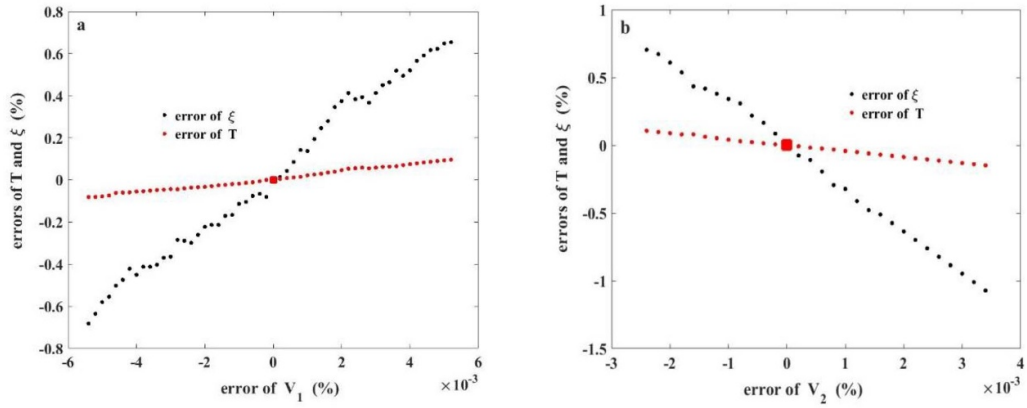

Figure 7. Relative errors of ξ (86.9% CO_2 in gas mixtures 86.9% CO_2– 13.1% N_2) and T depend on the measurement errors of the acoustic velocity in figure 6. (a) V_1 at $f_1 = 4.667$ kHz. (b) V_2 at $f_2 = 40$ kHz.

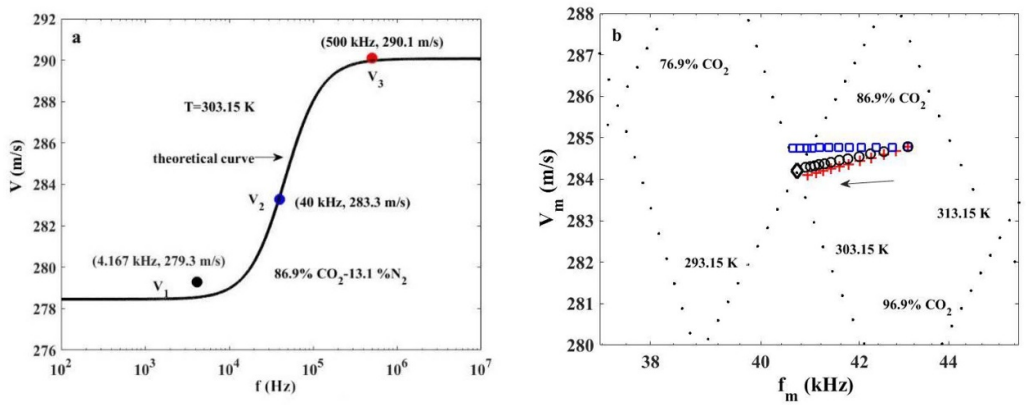

Figure 8. Measured velocities for reconstructing acoustic velocity dispersion are compared with the theoretical dispersion. (a) Symbol '•': measured V_1 with error, measured V_2 and V_3 without errors. Black curve: theoretical curve by our model. (b) Correction processes based on temperature. Symbol black '◯', blue '□', and red ' +': traces of corresponding inflection points from the reconstruction velocity dispersions by correcting V_1, V_2 and V_3; symbol '◊': theoretical inflection point. The points where black '◯', blue '□' and red ' +' are superimposed: inflection point of velocity dispersion reconstructed by V_1, V_2 and V_3 in figure 8(a).

lute error of 0.2% is more accurate. More importantly, Hu *et al* [15] only discussed the cases where the measured data must be lower than the theoretical value at low frequency and higher than the theoretical value at high frequency. However, our correction method does not require such severe correction conditions.

Table 5. Temperature correction results of inflection points from acoustic velocity dispersion reconstructed by single measurement error: gas mixture 86.9% CO_2–13.1% N_2 at 303.15 K.

Measurement error source	Final location of inflection point	Final temperature	Final composition	Absolute error for CO_2
$V_1 = 279.3$ m s^{-1}	$f_m = 47.19$ kHz,$V_m = 284.21$ m s^{-1}	303.6 K	86.9%CO2– 13.1%N2	0.0%
$V_2 = 283.3$ m s^{-1}	$f_m = 46.56$ kHz,$V_m = 284.75$ m s^{-1}	302.8 K	86.8%CO2– 13.2%N2	0.1%
$V_3 = 290.1$ m s^{-1}	$f_m = 47.29$ kHz,$V_m = 284.10$ m s^{-1}	304.4 K	86.7%CO2– 13.3%N2	0.2%

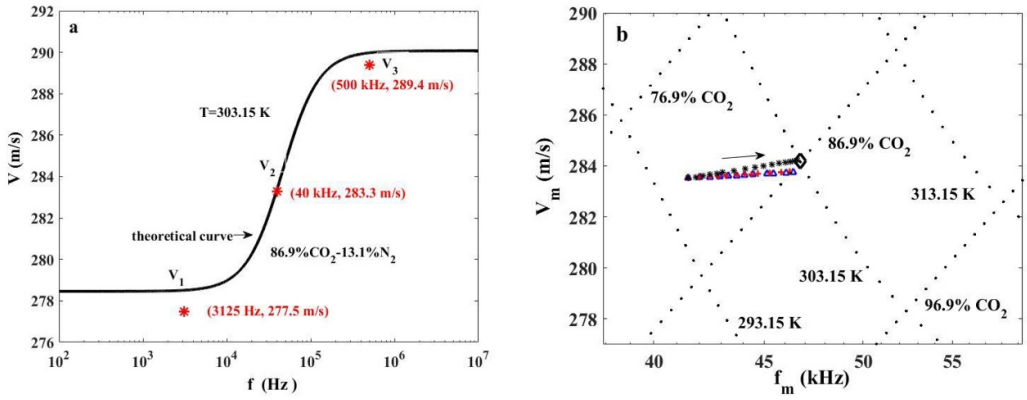

Figure 9. Measured velocities for reconstructing acoustic velocity dispersion are compared with the theoretical dispersion. (a) Symbol '*': measured V_1 and V_3 with errors, measured V_2 without error; black curve: theoretical curve by our model. (b) Correction processes based on temperature. Symbol black *, red+, and blue △: traces of corresponding inflection points from the reconstruction velocity dispersions; symbol '◇': theoretical inflection point. The points where symbol black *, red+, and blue △ are superimposed: inflection point of velocity dispersion reconstructed by V_1, V_2 and V_3 in figure 9(a).

Table 6. Temperature correction results of inflection points from acoustic velocity dispersion reconstructed by two measurement errors: gas mixture 86.9% CO_2–13.1% N_2 at 303.15 K.

Measurement error source	Final location of inflection point	Final temperature	Final composition	Absolute error for CO_2
V_1 and V_3	$f_m = 46.61$ kHz,$V_m = 284.21$ m s^{-1}	302.9 K	86.8%CO2– 13.2%N2	0.1%
V_2 and V_3	$f_m = 46.43$ kHz,$V_m = 283.75$ m s^{-1}	301.9 K	87.1%CO2– 12.9%N2	0.2%
V_1 and V_2	$f_m = 46.26$ kHz,$V_m = 283.87$ m s^{-1}	302.4 K	86.9%CO2– 13.1%N2	0.0%

5. Conclusion

In this paper, we demonstrated that the inflection point of acoustic velocity dispersion is related to molecular relaxation, and proposed a method to detect gas mixtures with similar, or even the same, sound speeds based on the locations of their inflection points. The inflection point can be synthesized from acoustic velocity dispersion by only measuring the acoustic velocity. To distinguish the gas composition, detection areas are constructed by a mixed relaxation model, and the detection error is effectively eliminated by the temperature correction function.

Traditional methods identify gas mixtures by sound speeds, which are invalid to gas mixtures with the same molar mass, but our proposed method can overcome the traditional problem and synthetically obtain both molar mass and relaxation information to distinguish them. Furthermore, the classical absorption becomes very large in the MHz frequency range, and the corresponding relaxation absorption of gases is so small that it is indistinguishable from noise. Thus, locating the inflection point for gas sensing is not only a simple method, but also the only approach applicable above the MHz frequency range for acoustic relaxation technology. Consequently, the proposed method has the potential to monitor gas mixtures in industry.

Acknowledgments

This work was supported by the National Key Technologies R&D Program of China (Grant No. 2016YFC0201101), the National Natural Science Foundation of China (Grant Nos. 61571201, 61701354 and 61873322), and the Program for Science & Technology Innovation Talents in Universities of He'nan Province (Grant No. 18HASTIT022).

ORCID iD

Ming Zhu https://orcid.org/0000-0001-5007-3919

References

[1] Chamorro C R, Segovia J J and Villaman M A 2006 Speeds of sound in (1-*x*)CH4+*x*N2 with $x = (0.10001, 0.19999$ and

0.5422) at temperatures between 170 K and 400 K and pressures up to 30 MPa *J. Chem. Thermodyn.* **38** 929–37
[2] Polturak E, Garrett S L and Lipson S G 1986 Precision acoustic gas analyzer for binary mixtures *Rev. Sci. Instrum.* **57** 2837–41
[3] Tinge J T, Mencke K, Bosgra L and Drinkerbury A A H 1986 Ultrasonic gas analyser for high resolution determination of binary-gas composition *J. Phys. E: Sci. Instrum.* **19** 953–6
[4] Vyas J C, Katti V R, Gupta S K and Yakhmi J V 2006 A non-invasive ultrasonic gas sensor for binary gas mixtures *Sens. Actuators.* B **115** 28–32
[5] Lueptow R M and Phillips S 1994 Acoustic sensor for determining combustion properties of natural gas *Meas. Sci. Technol.* **5** 1375–81
[6] Sebtahmadi S S, Yaghmaee M S, Raissi B, Riahifar R and Javaheri M 2019 General modeling and experimental observation of size dependence surface activity on the example of Pt nano-particles in electrochemical CO gas sensors *Sens. Actuators.* B **285** 310–6
[7] Ren W, Luo L and Tittel F K 2015 Sensitive detection of formaldehyde using an interband cascade laser near 3.6 μm *Sens. Actuators.* B **221** 1062–8
[8] Li C, Dong L, Zheng C and Tittel F K 2016 Compact TDLAS based optical sensor for ppb-level ethane detection by use of a 3.34 μm room-temperature CW interband cascade laser *Sens. Actuators.* B **232** 188–94
[9] Witschi H 2000 Fritz Haber: 1868–1934 *Toxicol. Sci.* **55** 1–2
[10] Garrett S 2008 Sonic gas analyzer for hydrogen and methane *J. Acoust. Soc. Am.* **123** 3372
[11] Hallewell G, Crawford G, McShurley D, Oxoby G and Reif R 1988 A sonar-based technique for the ratiometric determination of binary gas mixtures *Nucl. Instrum. Methods Phys. Res.* A **264** 219–34
[12] Zipser L and Wächter F 1995 Acoustic sensor for ternary gas analysis *Sens. Actuators.* B **26–27** 195–8
[13] Herzfeld K F and Litovitz T A 1959 *Absorption and Dispersion of Ultrasonic Waves* (New York: Academic Press)
[14] Petculescu A and Lueptow R M 2012 Quantitative acoustic relaxational spectroscopy for real-time monitoring of natural gas: A perspective on its potential *Sens. Actuators.* B **169** 121–7
[15] Hu Y, Wang S, Zhu M, Zhang K, Liu T and Xu D 2014 Acoustic absorption spectral peak location for gas detection *Sens. Actuators.* B **203** 1–8
[16] Zhang K-S, Wang S, Zhu M and Ding Y 2013 Algorithm for capturing primary relaxation processes in excitable gases by two-frequency acoustic measurements *Meas. Sci. Technol.* **24** 055002
[17] Liu T, Wang S and Zhu M 2017 Decomposition of effective specific heat of molecular relaxation for gas detection in a mixture *J. Acoust. Soc. Am.* **141** 1844
[18] Liu T, Wang S and Zhu M 2017 Predicting acoustic relaxation absorption in gas mixtures for extraction of composition relaxation contributions *Proc. R. Soc.* A **473** 20170496
[19] Zhang X-Q, Wang S and Zhu M 2018 Acoustic rotational relaxation of hydrogen around normal temperature *Acta. Phys. Sin.* **67** 094301
[20] Zhang X, Wang S, Zhu M, Zhang K, Liu T and Peng G 2019 Decoupling multiple rotational relaxations of hydrogen to detect gas mixtures *IEEE Access* **7** 115774–82
[21] Phillips S, Dain Y and Lueptow R M 2003 Theory for a gas composition sensor based on acoustic properties *Meas. Sci. Technol.* **14** 70–75
[22] Zhu M, Liu T, Zhang X and Li C 2018 A simple measurement method of molecular relaxation in a gas by reconstructing acoustic velocity dispersion *Meas. Sci. Technol.* **29** 015109
[23] Ejakov S G, Phillips S, Dain Y, Lueptow R M and Visser J H 2003 Acoustic attenuation in gas mixtures with nitrogen: experimental data and calculations *J. Acoust. Soc. Am.* **113** 1871–9
[24] Petculescu A G and Lueptow R M 2005 Synthesizing primary molecular relaxation processes in excitable gases using a two-frequency reconstructive algorithm *Phys. Rev. Lett.* **94** 1–4
[25] Zhang K-S, Wang S, Zhu M, Ding Y and Hu Y 2013 Decoupling multimode vibrational relaxations in multi-component gas mixtures: analysis of sound relaxational absorption spectra *Chin. Phys.* B **22** 014305
[26] Petculescu A, Hall B, Fraenzle R, Phillips S and Lueptow R M 2006 A prototype acoustic gas sensor based on attenuation *J. Acoust. Soc. Am.* **120** 1779–82
[27] Bhatia A B 1985 *Ultrasonic Absorption: An Introduction to the Theory of Sound Absorption and Dispersion in Gases, Liquids,and Solids* (New York: Courier Corporation)
[28] Dain Y and Lueptow R M 2001 Acoustic attenuation in three-component gas mixtures theory *J. Acoust. Soc. Am.* **109** 1955–64
[29] Zhang K-S, Wang S, Zhu M, Hu Y and Jia Y-Q 2012 Analytical model for acoustic multi–relaxation spectrum in gas mixtures *Acta. Phys. Sin.* **61** 174301
[30] Montero S and Pérez-Ríos J 2014 Rotational relaxation in molecular hydrogen and deuterium: theory versus acoustic experiments *J. Chem. Phys.* **141** 114301
[31] Douglas Shields F 1970 On obtaining transition rates from sound absorption and dispersion curves *J. Acoust. Soc. Am.* **47** 1262–8
[32] Valley L M and Amme R C 1968 Multiple velocity dispersion in normal hydrogen and in normal hydrogen-helium mixtures *Acoust. Soc. Am. J.* **44** 1144–5
[33] Valley L M and Legvold S 1960 Sound dispersion in ethane and 1·1-difluoroethane *J. Chem. Phys.* **33** 627–9
[34] Trusler J P M and Zarari M 1992 The speed of sound and derived thermodynamic properties of methane at temperatures between 275 K and 375 K and pressures up to 10 MPa *J. Chem. Thermodyn.* **24** 973–91
[35] Estrada-Alexanders A F and Trusler J P M 1995 The speed of sound in gaseous argon at temperatures between 110 K and 450 K and at pressures up to 19 MPa *J. Chem. Thermodyn.* **27** 1075–89
[36] Estrada-Alexanders A F and Trusler J P M 1998 Speed of sound in carbon dioxide at temperatures between (220 and 450) K and pressures up 1.4 MPa *J. Chem. Thermodyn.* **30** 685–95
[37] Ewing M B and Trusler J P M 2000 Primary acoustic thermometry between $T = 90$ K and $T = 300$ K *J. Chem. Thermodyn.* **32** 1229–55
[38] Behnen S W, Rothwell H L and Amme R C 1971 Vibration-rotation energy transfer between CO 2 (ν 2) and orthohydrogen *Chem. Phys. Lett.* **8** 318–20
[39] Wong G S K 2002 *Handbook of the Speed of Sound in Real Gases* (New York: Academic)